



**HAL**  
open science

## A compact dust shell in the symbiotic system HM Sge

Stéphane Sacuto, Olivier Chesneau, Martin Vannier, Pierre Cruzalèbes

► **To cite this version:**

Stéphane Sacuto, Olivier Chesneau, Martin Vannier, Pierre Cruzalèbes. A compact dust shell in the symbiotic system HM Sge. *Astronomy & Astrophysics - A&A*, 2007, 465, pp.469. 10.1051/0004-6361:20066642 . hal-00130854

**HAL Id: hal-00130854**

**<https://hal.science/hal-00130854v1>**

Submitted on 14 Feb 2007

**HAL** is a multi-disciplinary open access archive for the deposit and dissemination of scientific research documents, whether they are published or not. The documents may come from teaching and research institutions in France or abroad, or from public or private research centers.

L'archive ouverte pluridisciplinaire **HAL**, est destinée au dépôt et à la diffusion de documents scientifiques de niveau recherche, publiés ou non, émanant des établissements d'enseignement et de recherche français ou étrangers, des laboratoires publics ou privés.

# A compact dust shell in the symbiotic system HM Sge<sup>\*</sup>

S. Sacuto<sup>1</sup>, O. Chesneau<sup>1</sup>, M. Vannier<sup>2</sup>, P. Cruzalèbes<sup>1</sup>

<sup>1</sup> Observatoire de la Côte d'Azur, Dpt. Gemini-CNRS-UMR 6203, Avenue Copernic, F-06130 Grasse  
e-mail: [stephane.sacuto@obs-azur.fr](mailto:stephane.sacuto@obs-azur.fr)

<sup>2</sup> ESO, Alonso de Cordova 3107, Vitacura. Casilla 19001, Santiago 19, Chile.

Received; accepted

## ABSTRACT

**Aims.** We present high spatial resolution observations of the mid-infrared core of the dusty symbiotic system HM Sge<sup>\*\*</sup>.

**Methods.** The MIDI interferometer was used with the VLT Unit Telescopes and Auxiliary Telescopes providing baselines oriented from PA=42° to 105°. The MIDI visibilities are compared with the ones predicted in the frame of various spherical dust shells published in the literature involving single or double dusty shells intended to account for the influence of the hot White Dwarf.

**Results.** The mid-IR environment is unresolved by a 8m telescope (resolution~300 mas) and the MIDI spectrum exhibits a level similar to the ISO spectra recorded 10yr ago. The estimated Gaussian Half Width at Half Maximum of the shell of  $7.8\pm 1.3$  mas (12AU, assuming a distance of 1.5kpc) in the 8-9 $\mu$ m range, and  $11.9\pm 1.3$  mas (18AU) in the 11-12 $\mu$ m range, are much smaller than the angular separation between the Mira and the White Dwarf of 40 mas (60AU). The discrepancies between the HWHM at different angle orientations suggest an increasing level of asymmetry from 13 to 8 $\mu$ m. The observations are surprisingly well fitted by the densest (optically thick in the N band) and smallest spherical model published in the literature based on the ISO data, although such a model does not account for the variations of near-IR photometry due to the Mira pulsation cycle suggesting a much smaller optical thickness. These observations also discard the two shells models, developed in an attempt to take into account the effect of the White Dwarf illumination onto the dusty wind of the Mira. These models are too extended, and lead to a level of asymmetry of the dusty environment tightly constrained by the MIDI visibilities. These observations show that a high rate of dust formation is occurring in the vicinity of the Mira which seems to be not highly perturbed by the hot companion.

**Key words.** Techniques: interferometric; Techniques: high angular resolution; Stars: AGB and post-AGB; Stars: binaries: symbiotic; Stars: circumstellar matter; Stars: mass-loss

## 1. Introduction

HM Sge is a D-type (dust forming) symbiotic system that erupted as a symbiotic nova in 1975 (Dokuchaeva, 1976), evolving from a 17th to a 11th magnitude star with a rich emission line spectrum. The cool component is a Mira star and the hot component is a White Dwarf (WD) which had escaped detection enshrouded in the dense Mira envelop before this dramatic event.

HM Sge was observed in IR from the ground and also with the IRAS and ISO satellites. The observations show a spectrum dominated by silicate dust whose flux evolved deeply in about 30 yrs. Many papers investigated the time variable dusty environment and tried to evaluate the impact of the temperature and luminosity evolution of the WD on the dust (Dokuchaeva, 1976; Wenzel, 1976; Ciatti et al., 1977; Davidson et al., 1978; Ciatti et al., 1978; Kwok & Purton, 1979; Bryan & Kwok, 1991; Yudin et al., 1994; Bogdanov & Taranova, 2001; Schild et al., 2001). The

strong infrared excess detected shortly after the outburst indicates the presence of a rather dense dust envelope. The dust content of the system was severely affected by the nova outburst and it was soon observed that a process of dissipation of the dust was on the way (Taranova & Yudin, 1982, 1983), despite some obscuration events (Munari & Whitelock, 1989). The IRAS spectrum obtained in 1983 is about twice the ISO spectra obtained in 1996-1997 and this flux difference was attributed to a long-term variation effect and not to a beam size variation. Bogdanov & Taranova (2001) attributed these changes to an increase of the concentration and decrease of the temperature of the dust close to the Mira star, associated with the temperature increase and luminosity decrease of the White Dwarf. In the other hand, Schmid et al. (2000) find that the red giant spectrum has strongly brightened and find that the dust column in the line of sight has markedly decreased. It is difficult to assess whether this is a long-term evolution or an other event related to the presumably patchy circumstellar environment. This last hypothesis is favored by Schmid et al. (2000) and it must be noticed that longer wavelength emission is less sensitive to the clumpiness of the environment which probably implies that the conclusions of Bogdanov & Taranova (2001) and Schmid et al. (2000) are not necessarily incompatible.

Classically, most of the studies evaluated the infrared excess by fitting model spectral energy distributions (SEDs)

Send offprint requests to: S. Sacuto

\* Based on observations made with the Very Large Telescope Interferometer at Paranal Observatory under programs 075.D-0484 and 077.D-0216

\*\* Reduced visibilities and differential phases are available in electronic form at the CDS via anonymous ftp to [cdsarc.u-strasbg.fr](ftp://cdsarc.u-strasbg.fr) (130.79.128.5) or via <http://cdsweb.u-strasbg.fr/cgi-bin/qcat?J/A+A/>

hal-00130854, version 1 - 14 Feb 2007

to the instantaneous observed ones. The common model is a single dust shell, whose composition is dominated by silicates (but some studies involve a contribution from carbon (Bryan & Kwok, 1991)). However, this simple geometry could be considered as a crude approximation of a putatively complex geometry and dust composition of the mid-IR emitting regions. As an attempt to overcome this problem, more complex models involving two shells were used: a cool one surrounding the Mira star and a second, more extended that sees mostly the WD flux (Bogdanov & Taranova, 2001; Schild et al., 2001). The best argument for a two shell model is that the dust-rich area emission is affected by the combined effects of a ionizing UV irradiation from the hot primary on the expanding dust shell of the red giant, and a compression wave of the colliding winds in the transition zone. The conclusions of such approaches appear in contradiction to each other: whereas Schild et al. (2001) found a better match of the data with a two-component model of dust distribution, Bogdanov & Taranova (2001) are lead to the opposite conclusion and claim that current models with only a single Mira-type source are preferable. It is important to notice that both studies use the same ISO spectra as constraints and that they are able to provide satisfactory fits of the SED with very different model parameters. It is obvious that the single constraint of a SED is not able to fully constrain a putatively complex dust environment whose composition, geometry and even the luminosity of the heating sources is poorly known. An additional difficulty is that the mid-IR observations are to date scarce and secured only with relatively extended beams. Moreover, HMsge is not in an equilibrium state (Mira pulsations, wind interactions, dissipation/formation of obscuring dust,...) and this picture might well have evolved over the past few years since the ISO observations in 1996-1997. There is also a need for a SED taken with a much smaller beam than the ISO one which would allow to isolate the signature of the most recently formed dust.

We present in this article the first mid-infrared interferometric observations of this system taken with the MIDI/VLTI instrument recorded in 2005/2006 providing a spectrum update from a 8m telescope beam (FWHM $\sim$ 300mas) and a 1.5m telescope beam (FWHM $\sim$ 1.5''), and measurements of spatially correlated flux in interferometric mode that provide high spatial resolution ( $\sim$ 20 mas) and multi-spectral ( $\lambda/\Delta\lambda \sim 30$ ) information on the mid-IR source. The flux of VLT single dish spectrum is directly comparable to the the ISO ones (see Fig. 1). This is a clear indication that, first, most of the ISO emission observed 8yr before probably originated from a spatially compact region and second, that the dust content of the system seems not to have changed significantly. As a consequence, we assume in the following study that the spatial distributions expected from the different models developed by Schild et al. (2001) and Bogdanov & Taranova (2001) can be checked against these high spatial resolution observations and that the MIDI spectrum can be complemented with the ISO spectra to construct the current SED of the system at longer infrared wavelengths. The outline of the paper is the following: we present first the MIDI observations in Sec.2 and we summarize the published parameters of the models developed by Schild et al. (2001) and Bogdanov & Taranova (2001) in Sec.3. Then in Sec.4, the expected visibilities from the models are compared to the MIDI observations (the detail of the calculations is shown

in appendix). We propose some improvements for the best model in Sec.5. We discuss the limitations of the approach based on spherically symmetric dust shells for the study of a spatially complex source in Sec.6. Finally we summarize and conclude in Sec.7.

## 2. Observations

The Very Large Telescope Interferometer (VLTI) of ESO's Paranal Observatory has been used with MIDI, the Mid-infrared Interferometric recombiner (Leinert et al., 2003). MIDI combines the light of two telescopes and provides spectrally resolved visibilities in the N band atmospheric window.

The observations of HMsge were conducted with the VLT Unit Telescopes (UTs) UT2, UT3 and UT4, providing projected baselines in the range of 32-59 meters and the Auxiliary Telescopes (ATs) E0 and G0, providing projected baselines in the range of 13.5-16 meters.

The UTs observations were made during the nights of July 23-24th 2005, May 17th 2006 and June 11th 2006. The phase of the Mira during the UTs MIDI observations was 0.75 in 2005 and between 0.31-0.36 in 2006 (Yudin et al., 1994). The data were recorded with different projected baselines, (46.5m, 44 $^\circ$ ), (32.1m, 42 $^\circ$ ), (37.8m, 47 $^\circ$ ), (46.2m, 47 $^\circ$ ), (59.3, 105 $^\circ$ ) and (46.8, 101 $^\circ$ ). The ATs observations were made during the nights of May 21th 2006, May 27th 2006 and June 16th 2006. The phase of the Mira during the ATs MIDI observations was between 0.32-0.37 in 2006 (Yudin et al., 1994). The data were recorded with different projected baselines, (13.5m, 80 $^\circ$ ), (15.8m, 69 $^\circ$ ), (15.8m, 75 $^\circ$ ) and (15.3m, 77 $^\circ$ ) but the night of May 21th 2006 was discarded due to the misalignment of the star (see below). All the observations were made under good atmospheric conditions ( $\overline{seeing} \sim 1.01''$ ) with the worst seeing ( $\sim 1.75''$ ) during the night of July 23th 2005<sup>1</sup>.

The data reduction softwares<sup>2</sup> MIA and EWS (Jaffe, 2004) were used to reduce the spectra and visibilities (Chesneau et al., 2005). Chopped acquisition images are recorded (f=2Hz, 2000 frames, 4 ms per frame, 98 mas per pixel) for the fine acquisition of the target. The acquisition filter was a N band filter. The prism of MIDI was used providing a spectral dispersion of about 30.

Tab. 1 presents the journal of the interferometric observations. The calibrators, HD188512 (G8IV, diam=1.98 $\pm$ 0.02mas), HD187642 (A7V, diam=3.22 $\pm$ 0.01mas) and HD206778 (K2Ib, diam=8.38 $\pm$ 0.09mas) were observed right before or after each science target observations.

The spectral template from Cohen et al. (1999) of HD180711 (G9III) was scaled to the 12 $\mu$ m flux of the interferometric calibrator HD188512 for absolute flux calibration. In interferometry, in parallel with measurements of the source, measurements of the nearby calibrator are taken. Because the difference in airmass did not exceed 0.1, no airmass correction was applied to the corrected spectra.

The MIDI spectrum compared to the ISO spectra taken at two different phases of the Mira is shown in Fig. 1. The

<sup>1</sup> The Adaptive Optics device MACAO dedicated to the VLTI provide diffraction limited images in N band for the UTs even for the worst condition encountered on this observation

<sup>2</sup> <http://www.mpia-hd.mpg.de/MIDISOFT/>, <http://www.strw.leidenuniv.nl/~nevec/MIDI/>

**Table 1.** Journal of observations: MIDI/UT2-UT3/UT3-UT4/E0-G0. The calibrators used to calibrate the visibilities are given below the science target. The phase of the Mira ( $\varphi_{Mira}$ ) during the observations is indicated. The length and position angle of the projected baseline are also indicated.

Star	UT date & Time	$\varphi_{Mira}$	Base[m]	PA [deg]
HM Sge	2005-07-23 06:48:42	0.75	46.5	44
HD188512	2005-07-23 07:12:10	-	-	-
HM Sge	2005-07-24 02:41:11	0.75	32.1	42
HD188512	2005-07-24 02:58:55	-	-	-
HM Sge	2005-07-24 03:42:18	0.75	37.8	47
HD188512	2005-07-24 04:03:14	-	-	-
HM Sge	2005-07-24 06:14:49	0.75	46.2	47
HD188512	2005-07-24 06:37:58	-	-	-
HM Sge	2006-05-17 09:04:02	0.31	59.3	105
HD187642	2006-05-17 09:27:14	-	-	-
HM Sge	2006-06-11 09:05:09	0.36	46.8	101
HD187642	2006-06-11 08:42:52	-	-	-
HM Sge	2006-05-27 08:17:39	0.33	15.8	75
HD206778	2006-05-27 08:39:57	-	-	-
HM Sge	2006-06-16 06:28:01	0.37	15.3	77
HD206778	2006-06-16 05:53:35	-	-	-

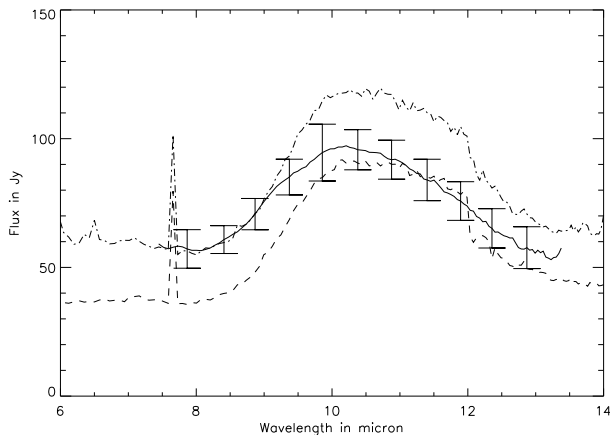


**Fig. 1.** The solid line with error bars is the MIDI flux (Mira pulsation phase,  $\varphi=0.75$ ) and the dashed and dashed-dotted lines are the ISO/SWS spectra (upper one: 1996,  $\varphi=0.65$ , bottom one: 1997,  $\varphi=1.08$ )

level of flux received by MIDI is equivalent to the flux level of ISO spectrum, implying that most of the N flux is concentrated within the 300mas beam of a 8m telescope and also that the level of emission has probably not significantly changed since the ISO observations (1996-1997). We notice that the flux error bars of the photometry from UTs are below 8% level. The shape of the silicate feature in the MIDI spectrum is different from that of the ISO spectra: the flux level at  $8\mu\text{m}$  is close to the upper ISO spectrum whereas the flux longward  $12\mu\text{m}$  is closer to the lower ISO spectrum. It is difficult to state whether this is due to the signature of

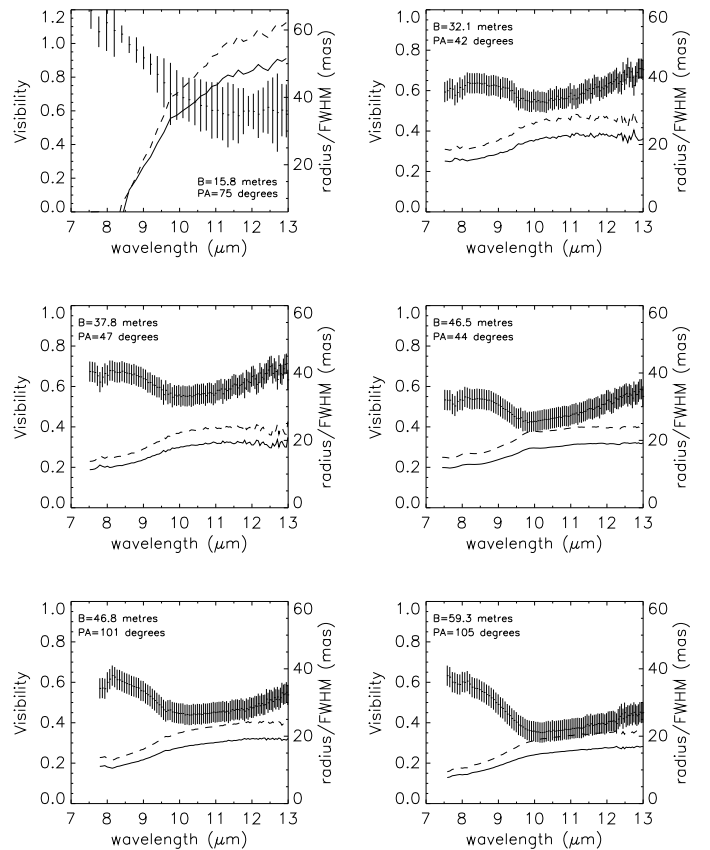


**Fig. 2.** MIDI visibilities (error bars) for the six projected baselines. The solid lines correspond to the uniform disk angular radius in mas and the dashed lines correspond to the FWHM in mas of the Gaussian distribution (both to be read from the scale on the right axis), computed from  $V$  at each wavelength.

the dusty source at this particular pulsation phase or the consequence of a longer term evolution.

We used all calibrators of each observing night to evaluate the quality of the calibration. The data were reduced with both MIA and EWS. For the UTs data, the quality is uniformly good and we decided to apply a uniform multiplicative error of 10% as a conservative estimate. The data reduction of the ATs data was much more difficult for several reasons: the alignment of the source was never optimal and strong biases in the extracted photometries were observed, affecting more the edges of the N band ( $7.5\text{-}9\mu\text{m}$  and  $12\text{-}13.5\mu\text{m}$ ). Moreover, the data reduction softwares are not currently optimized for these telescopes and developments are under way. As a consequence, we decided to show these data, but put only little weight on them compared to the more robust UTs data in the interpretation process. Some MIDI visibility curves were merged and averaged. We consider the two UTs observations of the July 23th 2005 at 06:48 and July 24th 2005 at 06:14 as approximately redundant because of their small baseline and position angle (PA) variation ( $<1\%$  and  $<7\%$ , respectively). This is also the case for the 2 ATs observations (May 27th 2006 and June 16th 2006) which have been averaged due to their small projected baselines and also their bad quality. The data from May 21th 2006 were disregarded due to alignment problems. The other ATs data were reduced, calibrated and

merged in a single curve in Fig. 2. We notice that the error bars at the edges of the N band, strongly affected by the photometric biases are probably underevaluated. The six remaining calibrated visibility data sets of HMsge over the wavelength range from  $7.5$  to  $13\mu\text{m}$  are shown in Fig. 2. The figure also shows the plot of the equivalent uniform-disk angular radius and FWHM of the Gaussian distribution calculated from the visibilities at each spectral channel. The size of both models increases from  $7.5$  to  $10\mu\text{m}$  and is approximately constant between  $10$  and  $13\mu\text{m}$ . Notice that the wavelength range has been slightly increased to show the MIDI visibilities between  $7$  and  $8\mu\text{m}$ , at the edge of the atmospheric window. The quality of the data is good, and we can see a decrease of visibility that corresponds to the very strong emission of the forbidden line [NeVI] at  $7.65\mu\text{m}$  (see Fig. 1). This narrow line is observed in the best quality MIDI spectra but almost disappeared in the mean spectrum presented in Fig. 1 due to small mismatch of the source position on the slit. This decrease can be interpreted as a much larger extension for the line emitting region. This is not investigated further in the paper due to the limited spectral resolution and the potentially large errors at this wavelength. Finally, all visibility and differential phase data as well as all the characteristics of the observations are available from the CDS (Centre de Données astronomiques de Strasbourg); all data products are stored in the FITS-based, optical interferometry data exchange format (OI-FITS), described in Pauls et al. (2005).

### 3. Spectrophotometric models

The infrared observations (mostly from IRAS and ISO) were interpreted within the frame of spherical models generated by the DUSTY package (Ivezić et al., 1999). We first reproduce the SEDs of models published by Schild et al. (2001) (S01) and Bogdanov & Taranova (2001) (B01). Then, still with the DUSTY code, we generate the corresponding synthetic spectrally-dispersed visibility profiles throughout the N band ( $7.5$ - $13\mu\text{m}$ ) and compare them with the MIDI visibilities for each baselines. The aims of our study are threefold: first, finding the model that provides the closest match with the data; second improving, if possible, the model parameters; and third, based on the best model, investigating a putative departure of spherical symmetry of the source.

#### 3.1. Description of the models

The models generated by S01 and B01 were based on the fit of the ISO SWS spectra of HMsge obtained in 10/01/1996 and 05/16/1997 (de Graauw et al., 1996; Salama et al., 1997). Assuming a period of the Mira variable of 527 days (Whitelock, 1987) and using the ephemeris of Yudin et al. (1994), they find that the observation were taken at phase 0.65 (i.e. shortly after the photometric maximum) and at phase 1.08, close to the MIRA minimum, respectively. Both studies consider single and double shell models generated with the DUSTY code. This public domain simulation code solves the problem of radiation transport in a circumstellar dusty environment by integrating the radiative transfer equation in plane-parallel or spherical geometries (Ivezić & Elitzur, 1996 a; Ivezić et al., 1999). The studies consider different a priori (fixed) input parameters:

- S01 :  $L_{cool}=5000L_{\odot}$  and  $L_{hot}=9200L_{\odot}$  luminosities considering the period-luminosity relation for Miras by Feast (1996) and the data of Murset et al. (1997), respectively. They also take a synthetic stellar spectrum for the Mira from Lejeune et al. (1997) with a temperature of 3000K and  $\log g=-0.29$ .
- B01 :  $L_{cool}=10600L_{\odot}$  and  $L_{hot}=9000L_{\odot}$  luminosities considering the period-luminosity relation obtained from observations of Mira oxygen stars in the Large Magellanic Cloud (Feast et al., 1989) and the relation of Murset & Nussbaumer (1994), respectively. They impose that the shell outer boundary associated with the Mira and the WD is situated at thousand times the inner boundary radius. Finally, they take into account a 2600K blackbody spectrum for the Mira.

Both authors consider a  $2\times 10^5$  K blackbody for the White Dwarf. In order to homogeneously compare the SEDs and visibilities of the models, we do not consider the synthetic stellar spectrum used by S01 and used a 3000K blackbody stellar spectrum for the Mira. The standard size distribution (MRN grain size distribution) as described by Mathis et al. (1977),  $n(a)\propto a^{-3.5}$  with minimum and maximum grain sizes of  $0.005\mu\text{m}$  and  $0.25\mu\text{m}$  respectively, and a chemical composition of warm silicate dust (W-Sil) with optical properties given by Ossenkopf et al. (1992), are also assumed by the 2 authors.

#### 3.2. Single shell models

The SED of single shell models are shown in Fig. 3. The corresponding dust shell output parameters given by the DUSTY code for S01 and B01 are listed in Tab. 2.

Although both models provide good quality SED fits, their parameters are very different. One important divergence comes from the inner boundary temperature of the shell. S01 find a temperature (1600K) close to the condensation temperature of the grains while B01 find a weaker temperature (700K). The inner radius from B01 is 8 times further than the one found by S01. The S01 visual optical depth is about twice larger ( $\tau_V=29$ ) than the one found by B01 ( $\tau_V=12.5$ ) with a dust density power law coefficient of 2.0 for B01 and 1.8 for S01. As a consequence, the S01 dust shell is more opaque than the B01 one, considering an identical dust chemical composition (warm silicate dust). B01 are satisfied with their single shell model whereas S01 think that the relatively high optical depth involved with their model ( $\geq 30$  mag) is not compatible with the JHK photometry by Kamath & Ashok (1999) suggesting that the light from the Mira is not highly absorbed in near-IR. For this reason, the single shell model is rejected by S01, with the additional argument that such a model is probably simplistic in view of the disturbing presence of the hot companion.

#### 3.3. Double shell models

Two shell models are an attempt to take into account the fact that each stellar component has its own effect on the dust generated in the Mira wind. The 2-component model can physically be justified with the scenario of a strong UV light source placed in the expanding shell of a red giant destroying the dust grains and generating an ionised nebula. Radiation pressure from the companion will secondly

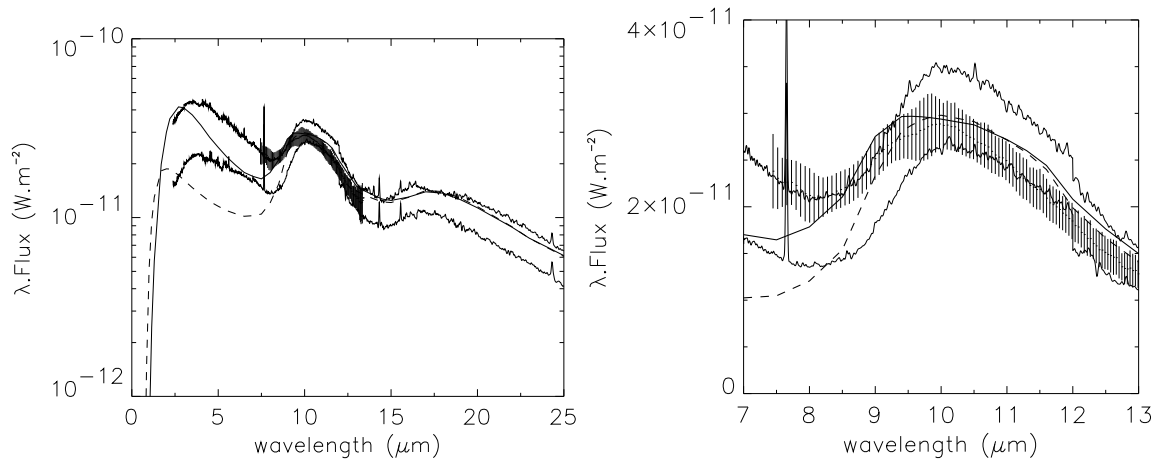


**Fig. 3.** Left: best fitting S01 single shell model (thick solid line) and best fitting B01 single shell model (thick dashed line), error bars correspond to the MIDI flux, both thin solid line are related to the ISO/SWS spectra. Right: close-up view of the best-fitted dust feature with the same labels.

**Table 2.** Summary of the single shell DUSTY fit of HMsge data. Values marked with an asterisk were pre-determined and fixed.

	Schild et al. (2001)	Bogdanov & Taranova (2001)
Effective temperature (K)	3000*	2600*
Luminosity ( $L_{\odot}$ )	5000*	10600*
Distance (kpc)	1.5	2.6
Central star diameter (mas)	1.6	1.8
Grain chemical composition	100% W-Sil*	100% W-Sil*
Grain size distribution	MRN*	MRN*
Density power law coefficient	1.8	2.0*
Inner boundary temperature (K)	1600	700
Geometrical thickness ( $r_{in}$ )	1000	1000*
Envelope inner radius (mas)	3.5	15.1
Visual optical depth	29	12.5
$10\mu\text{m}$ optical depth	2.47	1.77

slow the red giant wind and generate a compression wave in the transition zone in which the conditions for dust formation are very favorable, so that the thin dust rich layer can be identified with its structure. For sake of simplicity, both studies assume that none of the component heats the dust shell of the other and that the total emitted flux is a simple addition of the individual fluxes from each shell. The best parameters found by S01 and B01 are gathered in Tab. 3.

S01 combine the two dust shells with a partition factor  $p$  such that the observed flux:

$$F_{obs} = s(F_{WDShell} + pF_{MiraShell}) \quad (1)$$

where the scaling factor  $s$  converts the model flux at the distance of HMsge into the observed flux. One of the goals of the two shell modeling by S01 is to take into account the fact that the Mira in HMsge is optically observable, at least in the near-IR. Hence, they fix an a-priori visual optical depth range between 0.5 and 3.5, much lower than in the single shell hypothesis. The authors also impose that the dust shell thickness associated with the White Dwarf should be geometrically thin (i.e.  $Y_{out}/Y_{in} \leq 5$ ) and therefore could be approximated with a flat density distribution ( $x=0$ ). The parameters of this geometrical configuration (Tab. 3) consist in an optically thin, geometrically thick shell associated with the Mira, and a geometrically thin, optically thick shell associated with the White Dwarf. The

S01 2-component model is found satisfactory by Schild et al. (2001) but does not fit well shorter wavelengths dominated by the Mira spectrum. This can be attributed to the variability of the Mira which is not taken into account by the model. Despite some discrepancies, the authors favor the 2-component models approach. Fig. 4 shows their two shell best fitted model. The top-left part shows the S01 spectral energy distribution (SED) with the flux contribution of the individual shell, while its bottom-left part shows a close-up of the silicate dust peak around  $10\mu\text{m}$ .

The two shells model of B01 does not use any partition factor: it assumes that the flux from the central source is equal to the sum of two blackbodies located within a sphere of radius  $r_{in}$ . They argue that, given the small distance between the components (i.e. 40 mas) compared to the size of their common dust envelope, this condition is approximately satisfied. Contrary to the conclusion of S01, the results of the B01's study given in Tab. 3 lead the authors to conclude that the 2 shell model is unable to describe the observed energy distributions at mid-IR wavelengths due to a twice larger squared deviation comparing to the single shell model. Moreover, the distance is a free parameter of the model and B01 are lead to conclude that the overestimated distance values of the best fits (3.7kpc) is in contradiction with previous studies of HMsge. Fig. 4 shows their two shell best fitted model. The top-right part of Fig. 4 shows the B01 spectral energy distribution (SED)

with the flux contribution of the individual shell, while its bottom-right part shows a close-up of the dust peak around  $10\mu\text{m}$ .

We reproduce the models of Schild et al. (2001) and Bogdanov & Taranova (2001). It is very interesting to point out that the values of the parameters and their respective conclusions are in complete opposition, B01 favor a single shell model while S01 favor a two shell model. The extensions of the dusty shells are very different from one model to another, and our mid-infrared interferometry data bring an important constraint that can help us to disentangle between them.

## 4. Visibilities of the models

### 4.1. Description

In this section, we use DUSTY to generate the synthetic spectrally-dispersed ( $7.5\text{--}13\mu\text{m}$ ) visibility profiles for the 2 single shell and 2 double shell models of S01 and B01 for each projected baseline of the MIDI observations. Then we compare the synthetic visibilities with the mid-infrared visibility measurements recorded. More details on the computation of the synthetic visibilities with the DUSTY code can be found in Appendix A.

### 4.2. Single shell visibility models

Figure 5 shows the S01 (solid line) and B01 (dashed line) single shell visibility models superimposed on the MIDI visibilities (error bars) for each projected baseline. These plots show that, whatever the model, the visibilities are underestimated by comparison with the MIDI data. Nevertheless, the S01 model is relatively satisfactory, close to the observed visibilities, with a similar spectral shape. The B01 model provides much lower visibilities. We point out that the visibility curve shape of the S01 model is purely related to the chemistry of the shell and not a consequence of the geometry of the source. The drop of visibility at  $10\mu\text{m}$  is the consequence of the silicate emission, leading to a more extended object at these wavelengths (Chesneau et al., 2005). By contrast, the shape of the visibility curves from the B01 model depends on the projected baseline with the wavelength of minimum visibility changing from  $9.2$  to  $10\mu\text{m}$ . The shape of the B01 visibility curve reflects the change of angular diameter due to the silicates, but also the modulation of the visibility due to the ring resolved by the interferometer. The inner radius of the B01 model is large (angular diameter of  $30\text{mas}$ ), and the dust shell is rather optically thin ( $\tau_{10\mu\text{m}}=1.8$ ). Therefore, the dust emission is seen dominantly as a ring at low visibility level, whereas the S01 model is mostly seen as a compact source. Such modulations from an extended dusty ring have already been observed with MIDI (Chesneau et al., 2006).

The shape of the observed visibility curves is relatively constant, because the shell is optically thick or because the inner rim radius is too small to be resolved by the interferometer. The S01 model fulfills these two conditions: the  $10\mu\text{m}$  optical depth of the shell is  $2.5$ , and the angular diameter of the inner rim is only  $7\text{mas}$ .

Overall, the S01 model is impressively good, keeping in mind that the SED fits are usually not unique, and do

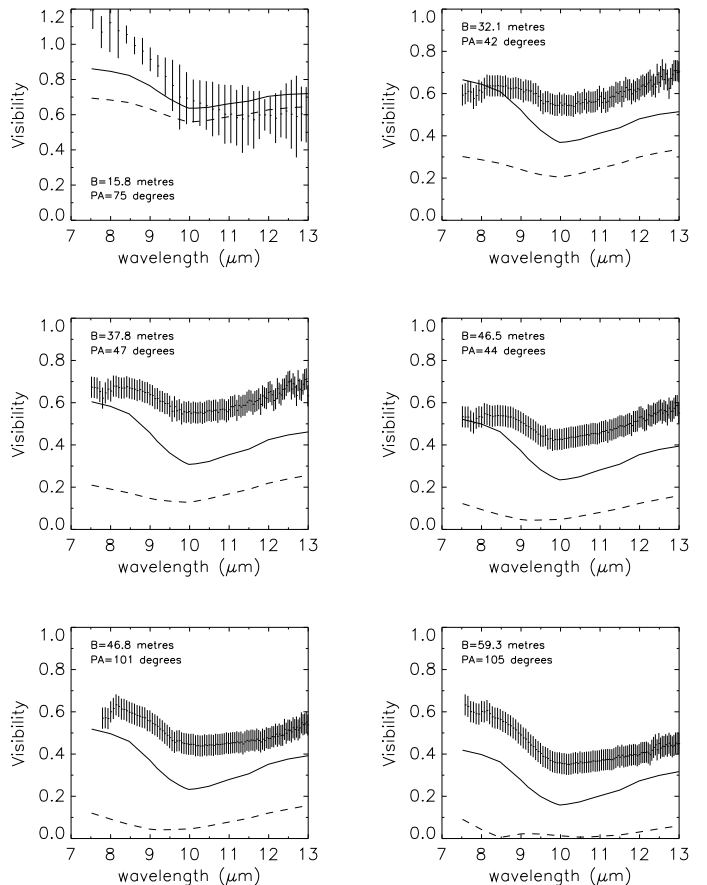


**Fig. 5.** Corresponding S01 (solid line) and B01 (dashed line) single shell visibility models superimposed on the MIDI visibilities (error bars) for the six projected baselines.

not provide good predictions for the observed radii of dust emission.

### 4.3. Double shell visibility models

Computing the contribution from two separate shells and adding them to form a resulting SED with the DUSTY code is a simple operation provided that the fluxes are supposed to be independent. This strong hypothesis is not viable in the context of our interferometric observations that are also sensitive to the relative position of the two shells. Hence, it is necessary to add to the description of the two shells their projected separation and position angle of their centers. Several options are possible: we position the centers of the two shells at the same position, or we position the centers at a given position and consider them as fixed parameters, or we consider these new parameters as free and part of the fitting process. In order to limit the extent of the current study, we fixed the parameters to the values of the binary found in Eyres et al. (2001): the Mira and WD shells are positioned  $40\text{mas}$  apart at a PA of  $130^\circ$ . The detailed visibility computation is given in Appendix B.

The direct consequence of the introduction of an extended shell in the two components models is a significant decrease of the N band visibilities of the S01 and B01 model. In addition, some differences in the shape of the visibility curves can be noticed (see Fig.6). The shapes of the visibilities of the B01 model exhibit a strong dependency on

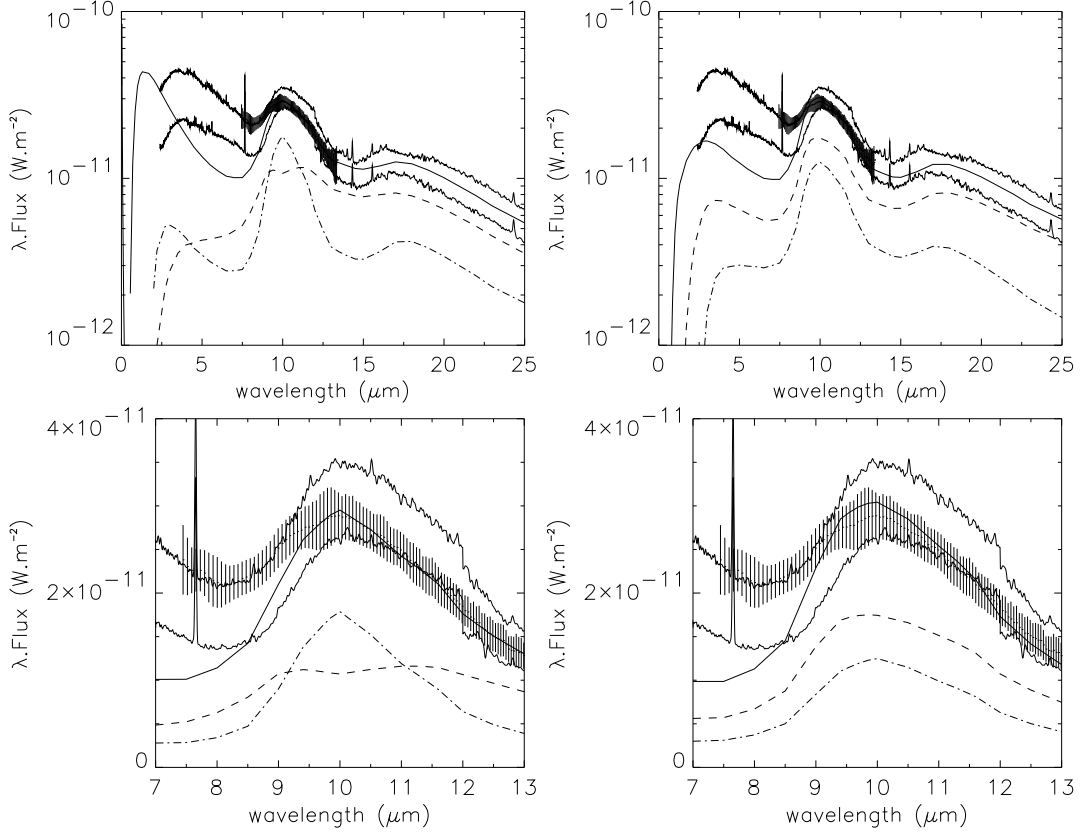


**Fig. 4.** Top-left: best fitting S01 two shell model (thick solid line). Top-right: best fitting B01 two shell model (thick solid line), the thin dot-dashed line is the flux contribution of the Shell M (associated with the Mira), the thin dashed line is the flux contribution of the Shell WD (associated with the White Dwarf), error bars correspond to the MIDI flux and both thin solid line are related to the ISO/SWS spectra. Bottom: close-up view of the corresponding best-fitted dust feature with the same labels.

**Table 3.** Summary of the two shell DUSTY fit of HMsge data. Shell "M" is the dust shell associated with the Mira component, Shell "WD" is the dust shell associated with the White Dwarf component. Values marked with a star were pre-determined and fixed.

	Schild et al. (2001)		Bogdanov & Taranova (2001)	
	M	WD	M	WD
Effective temperature (K)	3000*	$2 \times 10^5$ *	2600*	$2 \times 10^5$ *
Luminosity ( $L_{\odot}$ )	5000*	9200*	10600*	9000*
Distance (kpc)	1.5	1.5	3.7	3.7
Central star diameter (mas)	1.6	$5 \times 10^{-4}$	1.3	$2 \times 10^{-4}$
Grain chemical composition	100% W-Sil*	100% W-Sil*	100% W-Sil*	100% W-Sil*
Grain size distribution	MRN*	MRN*	MRN*	MRN*
Density power law coefficient	1.6	0*	2*	2*
Inner boundary temperature (K)	1400*	800	900	900
Geometrical thickness ( $r_{in}$ )	1000	1.1	1000*	1000*
Envelope inner radius (mas)	3.3	128.7	6.1	40.0
Visual optical depth	1.5	13	8.8	8.8
$10\mu\text{m}$ optical depth	0.13	1.11	0.75	0.75
Relative contribution	10	1	1	1

the position angle of the baseline. When the orientation of the projected baseline ( $\sim 45^\circ$ ) is perpendicular to the binary separation, i.e. the projected angular separation between the Mira and the WD is small ( $\sim 3.5$  mas for  $\text{PA} \sim 46^\circ$ ) compared to the spatial resolution of the interferometer (Fig.B.1), the spectral shape and the level of the visibilities are naturally explained by the predominant correlated flux from the Mira shell seen by the interferometer. The unique effect from the extended (over-resolved at baselines

larger than 30m) and optically thin ( $\tau_{10\mu\text{m}} = 0.75$ ) WD shell is to dilute the correlated flux to a low level with little spectral signature. When the orientation of the projected baseline gives a larger projected angular separation between the Mira and the WD ( $\sim 23$ -35 mas at  $\text{PA} \sim 75$ -100 $^\circ$ ) compared to the spatial resolution of the interferometer (Fig.B.1), the shift between the Mira and WD shells in the sky introduces an interferometric signal that mimics the one from a binary. Because the interferometer is able to resolve the



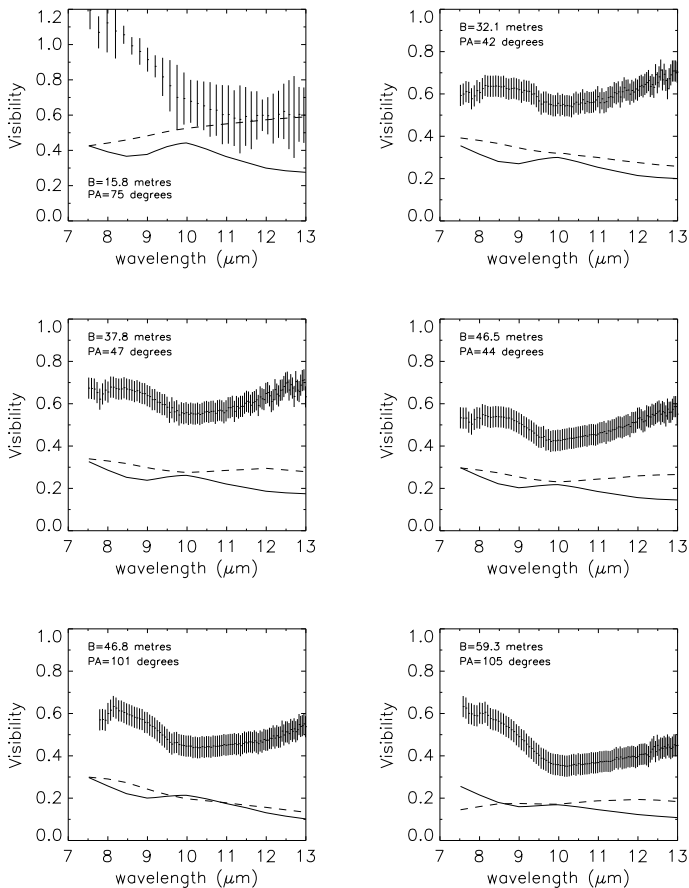


**Fig. 6.** Corresponding S01 (solid line) and B01 (dashed line) double shell visibility models superimposed on the MIDI visibilities (error bars) for the six projected baselines.

2 shells with their own photocenter, a variation occurs on the slope of the visibility depending on the projected baseline. The binary effect is given by a sinusoidal dependency of the visibility shape versus the projected angular separation of the 2 components. The visibility increases from 8 to  $13\mu\text{m}$  for the 15.8m baseline, then decreases for the 46.8m one, and increases again for the 59.3m one. This binary signal is not visible in the S01 model since the WD shell is over-resolved whatever the projected baseline and do not contribute to the correlated flux. The other differences between the shape of the S01 and B01 visibility curves come from the flux balance between the emission of the two shells at various wavelengths, as can be seen in Fig.4. The ratio of the two fluxes do not vary in the B01 model whereas a steep variation occurs between 9 and  $11\mu\text{m}$  in the S01 model. At  $9.7\mu\text{m}$ , the Mira shell dominates the flux leading to a local increase of the visibility.

Clearly it is debatable whether these dust shell models associating two *independent* flux sources and dust distributions are good approximations of complex sources as symbiotic novae and provide a better way of understanding them. More complex geometries should be used, constrained by hydrodynamical models and high resolution imaging, as a further step for improving our knowledge of these sources.

## 5. S01 single shell model improvement

In this section we consider the S01 single shell model as the potentially best model able to account for spectra and visibilities. We propose a pragmatic strategy of improvement that consists in small perturbations of the already satisfactory parameters of the S01 single shell model. We can see that the model is slightly too extended so that we need to spatially concentrate the emission of the dust shell.

A solution consists in playing with some intrinsic parameters of the dusty environment of HMsge, i.e. the density distribution power law and the optical depth. Steepening the density power law (at constant mass) increases the dust density at the inner boundary with the density dropping faster. The emission comes from a shell located closer to the inner boundary and, consequently, less resolved by the interferometer. A decrease of the optical depth (by decreasing the total amount of mass) leads to a more transparent dusty environment, so that deep seated layers contribute significantly to the correlated flux seen by the interferometer. These two changes do not affect the SED in the same way. The dust density distribution can only be constrained from the SED beyond  $10\mu\text{m}$  since the matter distribution mainly determines the slope of the re-distributed energy by dust emission (Lobel et al., 1999). On the other hand, a variation of the optical depth affects the whole shape of the curve, in particular the silicate feature. However, playing with both parameters, we find that the dust density distribution law has much more influence on the visibilities than a significant decrease of the optical depth. Moreover a decrease of the optical depth changes the whole SED curve that quickly does not fit the ISO and MIDI fluxes anymore. Diminishing the density power law coefficient increases the visibility but differences between the flux data and the model arise at longer wavelengths, with a too small flux of the model compared to the ISO data. It could be argued that this is due to the appearance of a beam size effect toward wavelengths larger than  $15\mu\text{m}$ , the ISO telescope gathering light from a large field-of-view. But the MIDI visibilities suggest a compact dusty environment that easily fits into the 8m telescope beam of 300 mas and the ISO emission is most probably also spatially compact at larger wavelengths.

The perturbed model has a density power law coefficient of 2.2 instead of 1.8 and a  $10\mu\text{m}$  optical depth of 2.15 instead of 2.47 with the remaining parameters equal to those of the S01 single shell (see Tab. 2). The fits are rather good but the optical depth of the perturbed model remains high. This model is subject to the same critics than for the S01 one: the shell prevents the flux from the Mira to be really detectable in near-IR. We tested a last change in order to improve the quality of the fits between 8 and  $10\mu\text{m}$ . One can notice that the model visibility slope between 8 and  $10\mu\text{m}$  is too strong revealing a too much extended structure at these wavelengths. Introducing a contribution from an optically thinner material than silicate such as carbon may allow to decrease the size of the object at these wavelengths.

Carbon in the form of graphite has been often involved to construct the early SED models (Kwok & Purton, 1979), and its presence was justified by the fact that this material would come from the White Dwarf ejecta during the outburst of 1975 or due to particular dust nucleation processes that occur under the non-equilibrium physical con-

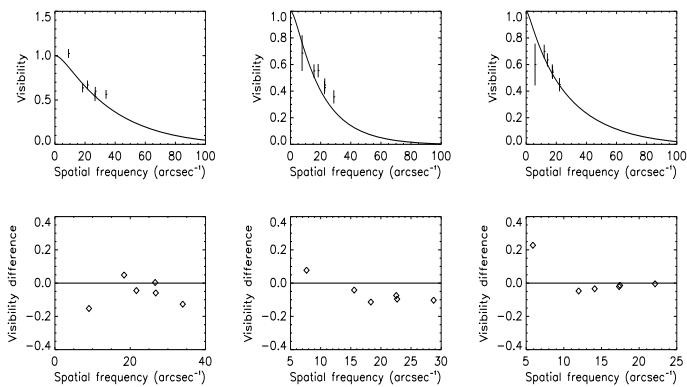


**Fig. 8.** Top: Best perturbed visibility profile model superimposed on the MIDI visibilities at 8.5, 10 and 13 $\mu\text{m}$  (from the left to the right). Bottom: Corresponding visibility difference between the model and the MIDI data.

ditions that prevail around the WD. Another argument is also provided by Bryan & Kwok (1991) in their analysis of the time variable 0.22 $\mu\text{m}$  feature in IUE spectra that they attribute to carbon-based material (see also Munari & Whitelock (1989)). If present, this carbon contamination must be small and we developed a test model in which the dust composition is a mixture of 90% of warm silicates (Ossenkopf et al., 1992) and 10% of amorphous carbon (Hanner, 1988). Fig. 7, shows the best perturbed S01 single shell model with the new mixture: the density power law coefficient is 1.8 and the 10 $\mu\text{m}$  optical depth has decreased to 1.89. The other parameters of this model keep the same values of the S01 model contained in Tab. 2. Fig. 8 shows the best perturbed visibility profile model superimposed on the MIDI visibilities at 8.5, 10 and 13 $\mu\text{m}$  and the visibility difference between the model and the MIDI data. Fig. 9 shows the corresponding best perturbed intensity profile model at the same wavelengths.

## 6. Discussion

### 6.1. Spherical models: single versus double shells

The main result of the MIDI observations is that the dust is spatially concentrated around the Mira star and that the MIDI single-dish fluxes is directly comparable to the ISO one. Using a Gaussian model, we estimated the HWHM of the dust in the 8-9 $\mu\text{m}$  and 11-12 $\mu\text{m}$  range to  $7.8 \pm 1.3$  mas (12AU) and  $11.9 \pm 1.3$  mas (18AU) respectively.

We compared the MIDI data with the predictions of various single and double spherical shells spectrophotometric models and favored the single shell models as they provided the most spatially concentrated emission. Gaussian model fitting of our best model provide the following Half Width at Half Maximum: 7.2 mas at 8.5 $\mu\text{m}$ , 13.2 mas at 10 $\mu\text{m}$ , and 11 mas at 13 $\mu\text{m}$  (see Fig. 9). These extensions are much smaller than the separation between the Mira and the WD of 40 mas (60AU) determined by the HST observations (Eyres et al., 2001). At 20 mas, the local intensity of the envelope is less than 3% than the one at 4 mas, and the amount of dust that is located in the vicinity of the WD is limited.

The mass-loss rates of the best S01 and the perturbed models are  $7.7 \times 10^{-6}$  and  $7 \times 10^{-6} M_{\odot}/\text{yr}$ , respectively. Similar estimations can be found in Richards et al.

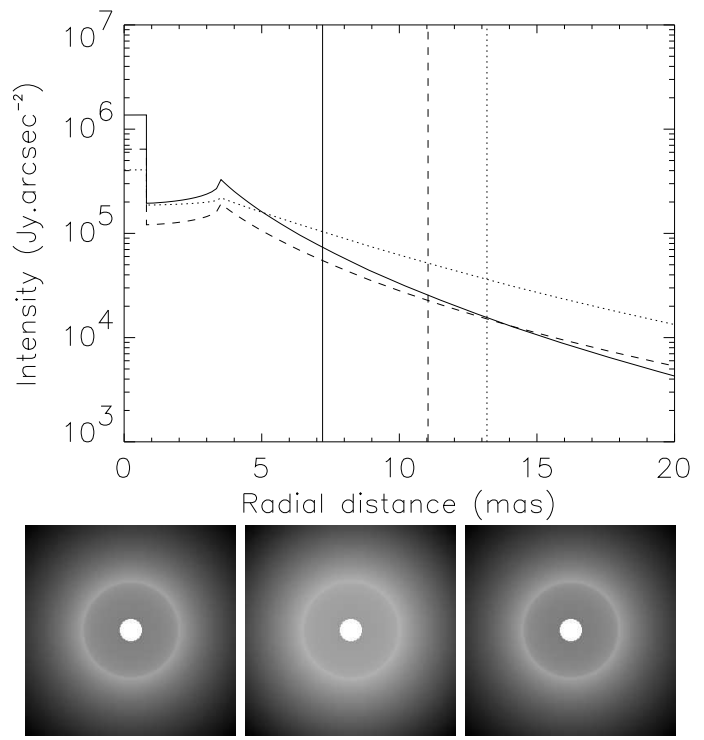


**Fig. 9.** Top: Best perturbed intensity profile model at 8.5 (solid line), 10 (dotted line), and 13 $\mu\text{m}$  (dashed line). The vertical lines indicate the HWHM (at 8.5 (solid line), 10 (dotted line) and 13 $\mu\text{m}$  (dashed line)) of the best perturbed intensity profile using a Gaussian fitting. Bottom: The mid-infrared images (at 8.5 (left), 10 (middle), and 13 $\mu\text{m}$  (right)) predicted by the best perturbed model given in a logarithmic scale.

(1999), Nussbaumer & Vogel (1990), and Kenyon & Garcia (1989).

The difficulty encountered in the fitting process is that a large amount of dust is required to explain the 10-100 $\mu\text{m}$  flux and that the Mira photosphere should be visible in the near-IR. The solution proposed by (Bryan & Kwok, 1991) is to use a large inner radius,  $10.5 R_{*}$  in the case of HMsge, but such a large inner radius would increase strongly the mid-IR extension of the system and is not compatible with the data. In the other hand, the best perturbed S01 model is able to fit many observations in first order but is still far from providing a satisfactory fit of the near-IR and long wavelength SED and is also too optically thick.

At this point, the main assumption of spherical symmetry has probably reached its limits. Although there is considerable evidence for departures from spherical symmetry at large scales ( $\geq 1''$ ), the primary constraints on the models from the MIDI mid-IR visibilities and spectra are not sufficient to warrant more complex models at small scales. The use of more complex models, like the one developed in Lopez et al. (1997) would help us to better constrain the dust density distribution of the system. However, such models have to be well defined through a large uv coverage and require a good knowledge of the wind-wind collision zone. We clearly lack this information with our limited data set and we consider this modeling out of the scope of the paper. Nevertheless, we investigate further whether any sign of departure from spherical symmetry of the mid-IR source

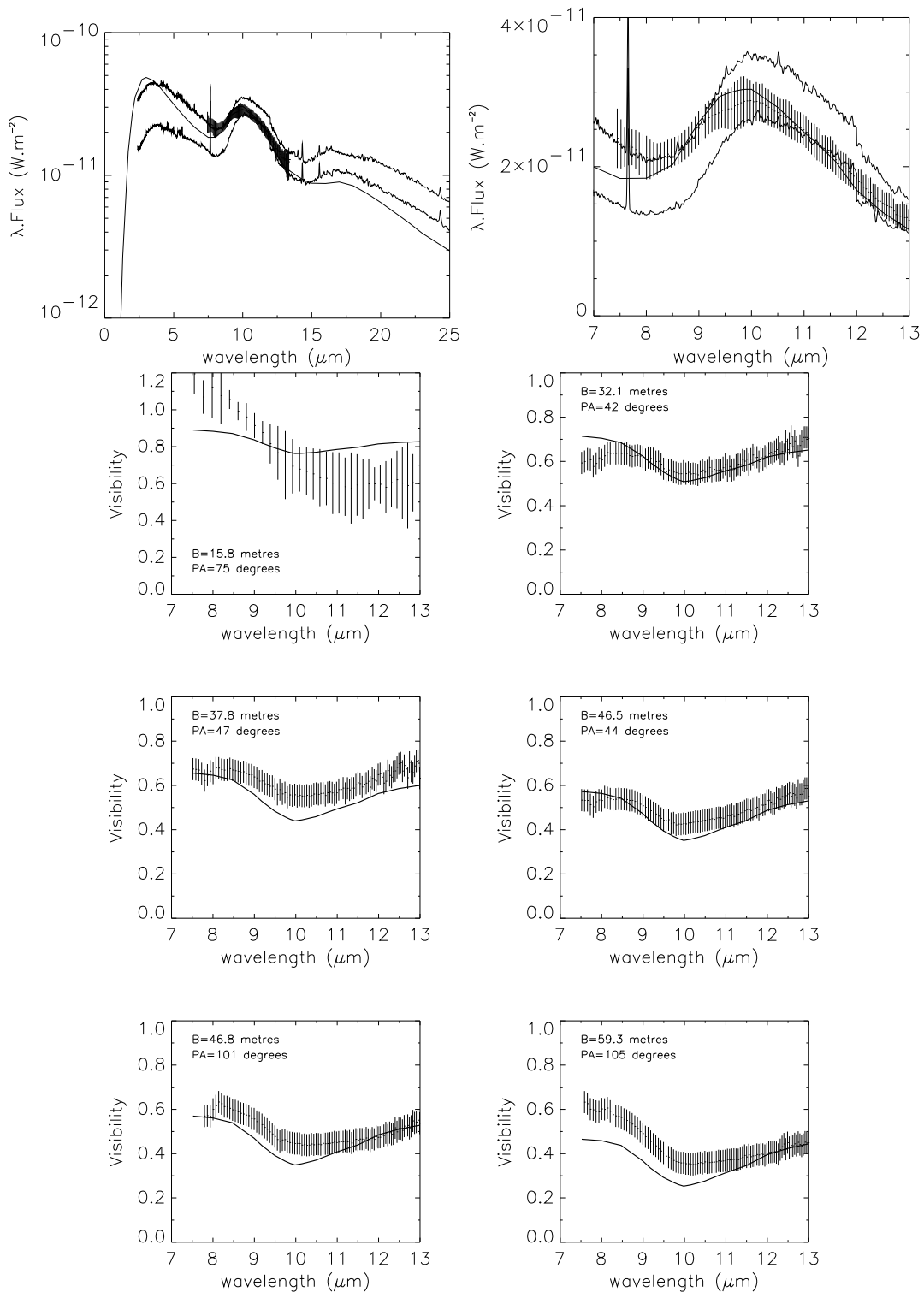


**Fig. 7.** Top-left: best fitting of the perturbed S01 single shell model (thick solid line), error bars correspond to the MIDI flux and both thin solid line are related to the ISO/SWS spectra. Top-right: close-up view of the best-fitted dust feature with the same labels. Bottom: Corresponding single shell visibility model superimposed on the MIDI visibilities (error bars) for the six projected baselines.

is seen by comparing the circumstellar dust extension according to the baseline orientation.

## 6.2. Departure from spherical symmetry

Our projected baselines cover position angles from  $42^\circ$  to  $105^\circ$ , allowing us to put some constraints on the degree of spherical geometry of the dust. It is also of prime importance to determine as best as possible whether a binary

signal is present in the MIDI data and whether the position angles of the projected baselines are aligned with a particular direction reported for the HMsge binary system from radio, optical or polarization data.

Let us recall first that even though the WD component has a high luminosity ( $\sim 10000L_{\odot}$ ) (Murset & Nussbaumer, 1994; Murset et al., 1997) and the binary system separation ( $\sim 40\text{mas}$ ) is optimum for a detection with the MIDI instrument, its low mid-IR flux prevents MIDI to directly detect its signal ( $F_{Nband}^{Mira}/F_{Nband}^{WD}\sim 10^5$ ). The mid-infrared flux coming from an accretion disk would add to the WD one, but the high temperature of such a structure makes it also too faint in mid-IR. The WD and a putative accretion disk could potentially perturb the dusty environment leading to a large scale signature mimicking a binary signal. Such a signal is probably observed in the case of R Aqr (Tuthill et al., 2000), that the authors attribute to a compact mid-IR source representing 3% of the N band flux<sup>3</sup> at 700 mas from the cool star (this separation would scale down to below 100 mas at 1.5kpc). Such a feature might be some localized concentration of dust, a local warming or a global asymmetry of the dust shell as also seen and discussed in Sec.4 in the frame of the B01 double shell model that predicts such a binary signature.

As previously said, the MIDI visibilities are rather smooth and no hint of such oscillation (as seen for instance in Chesneau et al. (2006)) is found in the data (the shape of the visibility profile may uniquely be related to the dust shell). It is possible to be more sensitive to a weak signal of this kind by using the differential phase. Fig. 10 shows the calibrated differential phase of the object evaluated from all the determined projected baselines (dotted lines). Error bars correspond to the rms of the differential phase over all the projected baselines. The rms values of the differential phase ( $\pm 4.26^{\circ}$  at  $8.5\mu\text{m}$ ,  $\pm 1.79^{\circ}$  at  $10.5\mu\text{m}$  and  $\pm 1.66^{\circ}$  at  $12.5\mu\text{m}$ ) indicates that there is no obvious signature of any astrophysical effects. The most discrepant curves are not correlated to a particular baseline length nor position angle and seem to reflect fast atmospheric changes during observations that were not fully corrected by the calibrator.

In order to estimate further the constraints provided by such measurements, we performed a perturbation of our best single shell model by a point-like structure at varying flux contrast, distance and angle. Our tests allow us to discard any compact mid-IR source representing more than about 1% of the total flux (i.e. 0.5 to 1 Jy between  $8\mu\text{m}$  and  $13\mu\text{m}$ ) at a distance ranging from 20mas to 80mas from the Mira star<sup>4</sup>.

Let us now consider the level of large scale asymmetry for the source. Fig. 11 shows the equivalent HWHM of the Gaussian intensity distribution according to the orientation of the projected baseline on the sky (UT2-UT3 and UT3-UT4). The figure is centered on the Mira and presents the binary axis direction (around  $120\text{-}130^{\circ}$  according to Eyres et al. (2001); Schmid et al. (2000)) located beyond the window at 40 mas north-west (Eyres et al., 2001). The MIDI baselines at  $\text{PA}\sim 45^{\circ}$  are oriented almost perpendicular to binary separation, in the direction of the outflows evidenced by various authors (Solf, 1984; Hack & Paresce,

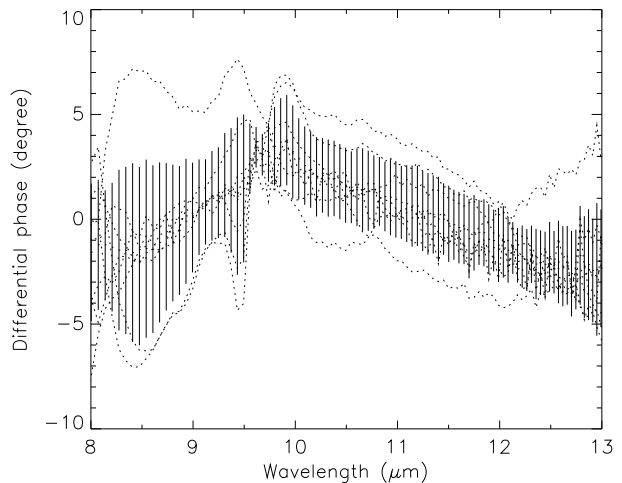


**Fig. 10.** Calibrated differential phase of the object evaluated from all the determined projected baselines (dotted lines). Error bars correspond to the rms of the differential phase averaged over all the projected baselines.

1993; Richards et al., 1999; Corradi et al., 1999; Eyres et al., 2001). On the contrary, the baselines at  $\text{PA}\sim 100^{\circ}$  are favorably oriented to probe the largest extension of the dust, if this dust is elongated in the preferential direction of the shadow of the Mira, that should efficiently protect the dust from the hard emission of the WD. The orbital period of HMsge is unknown but certainly rather long and we assume that it is barely unchanged since 1998, date of the latest polarization and HST observations<sup>5</sup>.

Using the Gaussian HWHM estimations, the following ratio between the HWHM at  $105^{\circ}$  and the ones at  $42^{\circ}$  can be computed at 8, 9, 10 and  $13\mu\text{m}$ , respectively:  $0.72_{-0.19}^{+0.32}$ ,  $0.80_{-0.17}^{+0.20}$ ,  $0.84_{-0.15}^{+0.19}$  and  $0.91_{-0.12}^{+0.14}$ . The extension of the shell is larger in the perpendicular direction than in the binary axis. The level of discrepancy is larger at  $8\mu\text{m}$  and steadily decreases toward longer wavelengths, with HWHM from 5 to 10 mas at  $8\mu\text{m}$ , to about 11 to 13 mas at  $13\mu\text{m}$ .

The wind from the cool star is likely to have an equatorial density enhancement. Spectro-polarimetric observations show that continuum from the Mira star is intrinsically polarized (Schmid et al., 2000) and this polarization would be, according to the author, most likely due to light scattering in an aspherical photosphere or wind.

Several geometries can be envisaged:

- A disk-like geometry seen almost edge-on. We expect to detect a strong difference between the MIDI visibilities with perpendicular baselines that is not observed. Moreover, depending on the inclination and the disk vertical extension, a large circumstellar absorption of the Mira light is expected.
- A disk-like geometry seen almost pole-on offer an elegant solution to the opacity problem: the light from the Mira star can reach us through an optically thin path whereas a dense and compact disk seen pole-on emits a

<sup>5</sup> We notice that the proper motions reported for some extended features in Richards et al. (1999) is typically  $2.5^{\circ}$  per year from north to east. If this estimation can be extrapolated to the binary motion, then the rough expected position angle of the projected binary plane should be around  $145\text{-}150^{\circ}$  at the time of the MIDI observations.

<sup>3</sup> Note that this signal is also seen in recent MIDI data.

<sup>4</sup> With a separation of 40mas, at full sinusoidal pattern should be seen in the spectrally-dispersed MIDI visibilities and differential phases from  $8\mu\text{m}$  to  $13\mu\text{m}$ .

large infrared excess. This geometry is relatively symmetrical and exhibit similar extensions whatever the direction of the baseline is.

- A slightly more complex geometry in which the Mira is wrapped into a shock cone (Fig.12) as presented in several studies Formigini et al., (1995); Mastrodemos & Morris (1999); Kenny & Taylor (2005). The density is not uniform and the envelop may be thinner (and patchy) in the direction perpendicular to the binary direction, allowing the Mira light to reach us, and a large dust content, mostly symmetrical to reside close to the Mira. This geometry is identical for pole-on or edge-on inclinations.

The probably high degree of symmetry of the source favors the two last scenario in which most of the dust resides in a spherical/disk-like pole-on envelope around the Mira, that is currently only slightly perturbed by the current hard flux of the WD. Such a low level of perturbation may appear surprising considering the strong uv source around the cool star, but the separation is rather large ( $\sim 60$ AUs), and the shielding of the uv flux by the dense and slow Mira wind is probably important (see the case of the symbiotic nebula PN M2-9 in Livio & Soker (2001)).

A continuum of inclinations is possible but the observations of a symmetrical optical and radio outflow suggest a high inclination. In the frame of the wind-wind collision geometry, the larger extensions perpendicular to the binary axes could be explained by a somewhat opened aperture angle of the shock cone. At  $8\mu\text{m}$ , hot dust emits preferentially close to the inner diameter of the Mira shell, but an additional emission component from the shock front may provide the asymmetry observed. As the contribution of the shock component decreases from 8 to  $13\mu\text{m}$ , the bulk of the emission is more centered around the Mira and the level of asymmetry decreases (see Fig.12).

We note that the wind-wind collision hypothesis has been investigated and modeled many times in the literature of HM Sge (Eyres et al., 2001; Richards et al., 1999; Girard & Willson, 1987; Willson et al., 1984a,b). The technique of mid-IR interferometry is a good opportunity to extensively study such a structure, but the present paper shows that two-telescopes observations, as currently performed by MIDI, are not sufficient to constrain its shape efficiently. What is clearly needed is an interferometric imager able to recombine simultaneously the light from the 4 UT or AT telescopes in the mid-IR. Such a recombiner called MATISSE is proposed for the second generation instrumentation of the VLTI (Lopez et al., 2006).

## 7. Summary and conclusion

We have presented new high spatial resolution observations of the dusty environment of HM Sge, consisting on MIDI/VLTI spectra and visibilities. Using the strong constraints provided by optical interferometry, we reassessed previous interpretations based only on the modeling of the spectral density distribution. In the case of the complex symbiotic systems, the spectral energy density can be modeled in different ways. Schild et al. (2001) and Bogdanov & Taranova (2001) have worked the same year on the ISO/SWS spectra of HM Sge. Both take into account single and double shell models, as an attempt to take into account the spatial complexity of the source. Both used the same

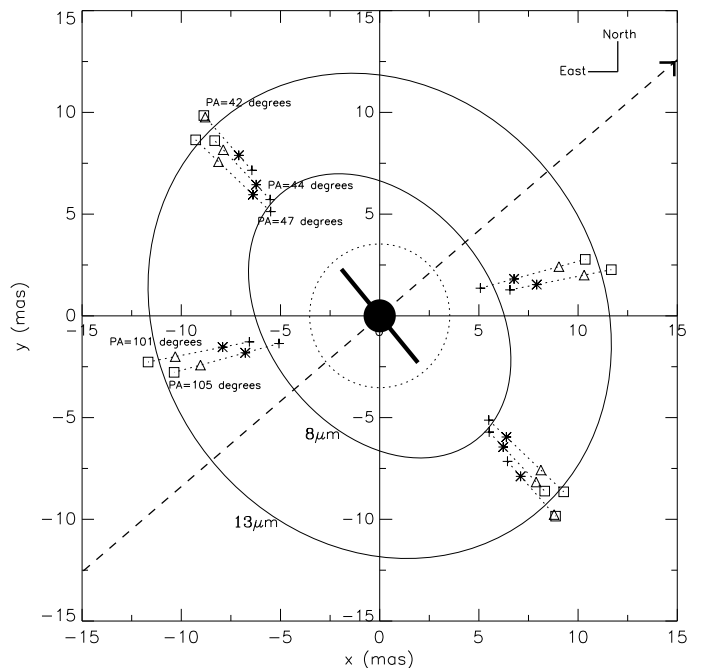


**Fig. 11.** Equivalent HWHM of the Gaussian intensity distribution (in mas) dependence on the projected baseline position angle on the sky. These HWHM are taken at 8 (plus), 9 (cross), 10 (triangle) et  $13\mu\text{m}$  (square). The figure is arbitrarily centered on the Mira and presents the binary axis (dashed line) ( $\text{PA}=130^\circ$ ) (Eyres et al., 2001) where the position of the White Dwarf at 40 mas (Eyres et al., 2001), represented by the arrow, is out of the window. The thick line, perpendicularly to the binary axis, represents the position angle of the Raman line polarization (Schmid et al., 2000). The black filled circle represents the dimension of the Mira determined with the best perturbed model. The dotted circle represents the dust shell inner boundary dimension determined with the best perturbed model. The two 8 and  $13\mu\text{m}$  solid ellipses have a minor axis of 5.6 and 11.1 mas, and a major axis of 7.8 and 12.5 mas, respectively.

radiative transfer code DUSTY. However, they do not converge to the same value of parameters and their respective conclusion are in complete opposition. The interferometric study of this object shows that the morphology of the dust was close enough to the single shell model of Schild et al. (2001) considering that the circumstellar environment of the symbiotic system was compact and optically thick (an angular inner radius of the dust shell located at 3.5 mas and a visual optical depth of 29).

An improvement of the model consisting in small perturbations of the Schild et al. (2001) parameters shows that a good fit of both SEDs and visibility curves is obtained steepening the density power law coefficient from 1.8 to 2.2 and decreasing the  $10\mu\text{m}$  optical depth from 2.47 to 2.15. The change of these two parameters gives a larger transparency of the circumstellar medium and allows the emission to come from deeper layers with the aim to spatially concentrate the emission of the dust shell. Finally the insertion of carbon material in the dusty layers allows to diminish a too much extended structure between 8 and  $10\mu\text{m}$ . Such a chemical component could come from the White Dwarf ejecta during the outburst of 1975 or from particular dust nucleation processes that occur under the

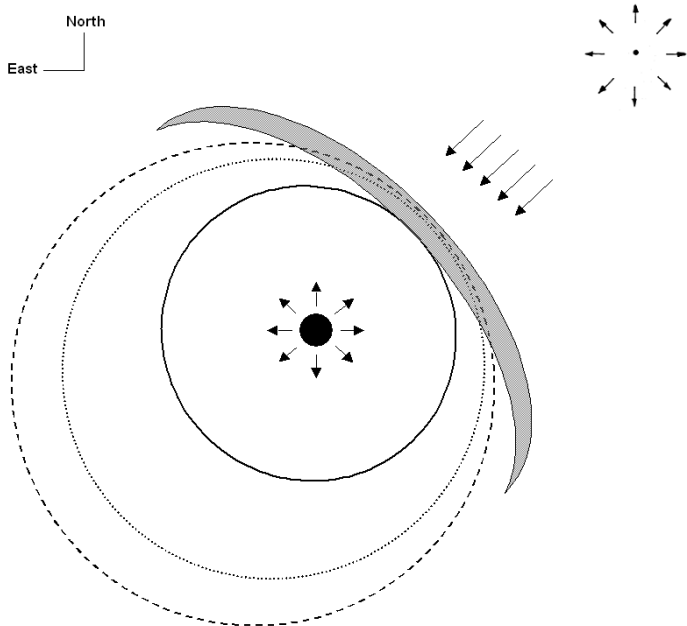


**Fig. 12.** Schematic representation of the symbiotic system in which the Mira (in the center of the figure) is wrapped into a shock cone. In the top on the right is the White Dwarf. The arrows surrounding the 2 components indicate the 2 winds and the parallel arrows symbolize the radiation reaching the shock front component (gray filled zone). The contribution of the shock component decreases from 8 to  $13\mu\text{m}$  simultaneously with the level of asymmetry. The 3 circular regions correspond to the dust shell extension at 8 (solid line), 10 (dotted line), and  $13\mu\text{m}$  (dashed line).

non-equilibrium physical conditions that prevail around the White Dwarf.

The compact model was rejected by Schild et al. (2001) because of its high optical depth not compatible with non-absorbed emission of the Mira in the near-IR. Our best spherical model has to face the same objection, but this issue could be solved assuming a more complex spatial distribution of the dust. Our MIDI data allowed us to investigate the departure of spherical symmetry using different baseline orientations. The extension is stronger in the direction perpendicular to the binary axis. This asymmetry is largest at  $8\mu\text{m}$  and steadily decreases toward longer wavelengths. We speculated on the origin of the departure. We propose that the Mira is wrapped into a shock cone where the density of the envelope is thinner and patchy in the direction perpendicular to the binary axis. This could allow the Mira light to reach us, and a large dust content, mostly symmetrical to reside close to the Mira. Further VLTI/MIDI observations at 15 different projected baselines with ATs are planned to confirm this geometrical scenario.

The MIDI observations must be included in the frame of the long-term evolution of the dusty envelope of HMsge associated with the variability of the conditions of dust survival in the system, and hence the luminosity and temperature of the White Dwarf, and also the relative position of the Mira and the WD in the orbit. The current dusty envelope from the Mira appears only slightly perturbed by the hot companion. As the time passes, the impact of the WD ionizing flux on the Mira dust shell should decrease further for this large separation binary system unless that

in the course of the putatively eccentric orbit a decrease of the separation occurs, or that a large accretion disk builds up.

*Acknowledgements.* Walter Jaffe and Rainer Köhler are warmly thanked for their constant efforts for improving the reducing software of MIDI, that contributes strongly to the success of the instrument. Without them, this study would not have been possible. Mr. Sacuto benefits from a PHD grant from the Conseil Régional Provence - Alpes - Côte d'Azur (FRANCE) managed by ADER-PACA.

## References

- Bogdanov, M.B. & Taranova, O.G., 2001, AZh, 78, 52  
 Bryan, G.L. & Kwok, S., 1991, ApJ, 368, 252  
 Chesneau, O. et al., 2005, A&A, 435, 275  
 Chesneau, O. et al., 2006, A&A, 455, 1009  
 Chochol, D. et al., 2004, CoSka, 34, 5  
 Ciatti, F. et al., 1977, A&A, 61, 459  
 Ciatti, F. et al., 1978, A&A, 68, 251  
 Cohen, M. et al., 1999, LPICo 969, 5  
 Corradi, R.L.M. et al., 1999, A&A, 348, 978  
 Davidson, K. et al., 1978 ApJ, 220, 239  
 de Graauw, T. et al., 1996, A&A, 315, 49  
 Dokuchaeva, O.D., 1976, IBVS, 1189, 1  
 Eyres, S.P.S. et al., 2001, ApJ, 551, 512  
 Feast, M.W. et al., 1989, MNRAS, 241, 375  
 Feast, M.W., 1996, MNRAS, 278, 11  
 Formigginì, L. et al., MNRAS, 277, 1071  
 Girard, T. & Willson, L. A., A&A, 183, 247  
 Hack, W.J. & Paresce, F. 1993, PASP, 105, 127  
 Hanner, M.S., 1988, NASA Conf. Pub., 3004, 22  
 IRAS Low Resolution Spectra (IRAS team, 1987)  
 Ivezić, Z. & Elitzur, M., 1996a, MNRAS, 279, 1011  
 Ivezić, Z., Nenkova, M., and Elitzur, M., 1999, User Manual for DUSTY  
 Jaffe, W.J., 2004, SPIE, 5491, 715  
 Kamath, U.S. & Ashok, N.M., 1999, A&AS, 135, 199  
 Kenny, H.T. & Taylor, A.R., 2005, AJ, 619, 527  
 Kenyon, S.J. & Garcia, M.R., 1989, AJ, 97, 194  
 Kwok, S. & Purton, C.R., 1979, ApJ, 229, 187  
 Kwok, S. et al., 1984, ApJ, 279, 188  
 Leinert, C. et al., 2003, Ap&SS, 286, 73  
 Lejeune, Th. et al., 1997, A&A Sup. Ser., 125, 229  
 Livio, M. & Soker, N., 2001, ApJ, 552, 685  
 Lobel, A. et al., 1999, A&A, 343, 466  
 Lopez, B. et al., 1997, ApJ, 488, 807  
 Lopez, B. et al., 2006, SPIE, 6268, 31  
 Mathis, J.S., Ruml, W., and Nordsieck, K.H., 1977, ApJ, 217, 425  
 Mastrodemos, N. & Morris, M., 1999, ApJ, 523, 357  
 Mueller, B.E.A. & Nussbaumer, H., 1985, A&A, 145, 144  
 Munari, U. & Whitelock, P.A., 1989, MNRAS, 237, 45  
 Murset, U. & Nussbaumer, H., 1994, A&A, 282, 586  
 Murset, U. et al., 1997, A&A, 319, 201  
 Nussbaumer, H. & Vogel, M., 1990, A&A, 236, 117  
 Ossenkopf, V. et al., 1992, A&A, 261, 567  
 Pauls, T.A. et al., 2005, PASP 117, 1255  
 Richards, A.M.S. et al., 1999, MNRAS, 305, 380  
 Salama, A. et al., 1997, Proc. of the First ISO workshop on analytical spectroscopy, ESA SP-419, 17  
 Schild, H. et al., 2001, A&A, 378, 146  
 Schmid, H.M. et al. 2000, A&A, 355, 261  
 Solf, J., 1984, A&A, 139, 269  
 Taranova, O.G. & Yudin, B.F. 1982, SvAL, 8, 46  
 Taranova, O.G. & Yudin, B.F. 1983, A&A, 117, 209  
 Tuthill, P. G. et al., 2000, ApJ, 534, 907  
 Wenzel, W., 1976, IBVS N, 1222  
 Whitelock, P.A., 1987, PASP, 99, 573  
 Willson, L. A. et al., 1984, A&A, 133, 137  
 Willson, L. A. et al., 1984, A&A, 133, 154  
 Yudin, H. et al., 1994, A&AS, 105, 169

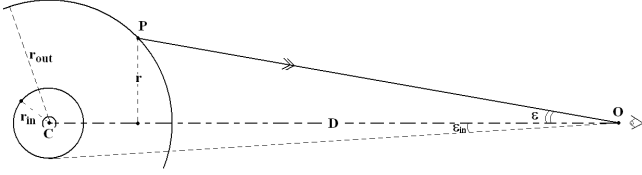


**Fig. A.1.** Geometry used for the determination of the emergent intensity from the shell outer boundary ( $P$ ) and received under the angle  $\varepsilon$  by the observer located at  $O$ , distant of  $D$  from the center  $C$  of the central source. The point  $r$  is the impact parameter;  $r_{in}$  is the inner boundary radius, and  $\varepsilon_{in}$  is the angular radius of the inner shell boundary.

## Appendix A: Determination of the model visibilities

The DUSTY code is used to get a theoretical model of the normalized radial intensity distribution at specified wavelengths. For each model, DUSTY provides the radial intensity (in  $\text{Jy.arcsec}^{-2}$ ) versus the invariant dimensionless reduced impact parameter  $\rho$  defined by

$$\rho = \frac{r}{r_{in}} \quad (\text{A.1})$$

where  $r$  is the impact parameter and  $r_{in}$  is the radius of the inner boundary (see Fig.A.1).

Taking into account that the star in the code is normalized at luminosity  $L_{\star}^D = 10^4 L_{\odot}$ , the radius  $r_{in}$  is given by

$$\frac{r_{in}}{r_{in}^D} = \sqrt{\frac{L_{\star}}{L_{\star}^D}} \quad (\text{A.2})$$

where  $r_{in}^D$  is the radius of the inner boundary when  $L_{\star}^D = 10^4 L_{\odot}$  and  $L_{\star}$  is the luminosity of the star.

Therefore, the impact parameter  $r$  is given by

$$r = \rho r_{in} = \rho r_{in}^D \sqrt{\frac{L_{\star}}{L_{\star}^D}} \quad (\text{A.3})$$

where the luminosity corresponds to the one given by the two authors for the Mira and the White Dwarf (see Tab.2 and Tab.3).

DUSTY also allows us to generate the theoretical visibility curves by calculating the Hankel transform of the circularly symmetric intensity distribution. The code gives the visibility versus the invariant dimensionless scaled spatial frequency  $\phi$  defined by

$$\phi = f \cdot 2\varepsilon_{in}, \quad (\text{A.4})$$

where  $f$  is the spatial frequency (in  $\text{arcsec}^{-1}$ ) and  $\varepsilon_{in}$  is the angular radius of the shell inner boundary (see Fig.A.1).

Taking into account that DUSTY considers a star with an observed bolometric flux  $F_{bol}^D = 10^{-6} \text{ W.m}^{-2}$ , the angular radius of the inner boundary is given by

$$\frac{\varepsilon_{in}}{\varepsilon_{in}^D} = \sqrt{\frac{F_{bol}}{F_{bol}^D}}, \quad (\text{A.5})$$

where  $\varepsilon_{in}^D$  is the angular radius of the inner boundary when  $F_{bol}^D = 10^{-6} \text{ W.m}^{-2}$  and  $F_{bol}$  is the observed bolometric flux of the source.

Therefore, the spatial frequency  $f$  is given by

$$f = \frac{\phi}{2\varepsilon_{in}} = \frac{\phi}{2\varepsilon_{in}^D} \sqrt{\frac{F_{bol}^D}{F_{bol}}}. \quad (\text{A.6})$$

DUSTY can produce maps of the visibility at up to 20 wavelengths. The visibilities of 20 spectral channels are generated between  $7.5$  and  $13\mu\text{m}$  corresponding approximately to the number of independent channel provided by MIDI with the low resolution mode (prism,  $R \sim 20$ ).

## Appendix B: The binary separation

In the frame of a two shell model, the relative position of the centers has to be taken into account in the computation of the visibilities. We adopted a binary separation and a position angle of the binary axis estimated of  $40 \text{ mas}$  and  $130^\circ$  respectively (Eyres et al., 2001). Putting the Mira star at the center of reference (see Fig.B.1), the expression of the visibility can be written as:

$$V = \frac{\sqrt{C_{tot} C_{tot}^*}}{F_{tot}} = \frac{\sqrt{C_M^2 + C_{WD}^2 + 2C_M C_{WD} \cos(2\pi \frac{B_I}{\lambda} \rho_0 \cos(\theta_I - \theta_0))}}{F_M + F_{WD}} \quad (\text{B.1})$$

where  $C_{tot}$  is the total correlated flux of the Mira plus the White Dwarf ( $C_{tot} = C_M + C_{WD} e^{-2\pi i \frac{B_I}{\lambda} \rho_0 \cos(\theta_I - \theta_0)}$ ) and  $C_{tot}^*$  is its conjugate.  $\vec{B} = (B_I; \theta_I)$  are the coordinates associated to the interferometer projected baseline on the sky where  $B_I$  is the baselength and  $\theta_I$  its position angle from the north to the east.  $\vec{\rho} = (\rho_0; \theta_0)$  are the coordinates associated to the binary components where  $\rho_0$  is the binary separation and  $\theta_0$  the position angle of the binary axis from the north to the east. Finally,  $F_{tot}$  represents the total flux of the Mira plus the White Dwarf ( $F_{tot} = F_M + F_{WD}$ ).

## List of Objects

- 'HM Sge' on page 1
- 'HM Sge' on page 1
- 'HM Sge' on page 1
- 'HM Sge' on page 1
- 'HM Sge' on page 2
- 'HM Sge' on page 2
- 'HD188512' on page 2
- 'HD187642' on page 2
- 'HD206778' on page 2
- 'HD180711' on page 2
- 'HD188512' on page 2
- 'HM Sge' on page 3
- 'HD188512' on page 3
- 'HM Sge' on page 3
- 'HD188512' on page 3
- 'HM Sge' on page 3
- 'HD188512' on page 3
- 'HM Sge' on page 3

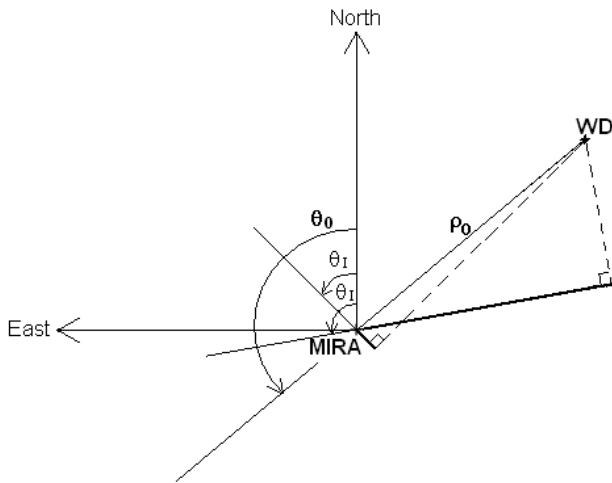


**Fig. B.1.** Schematic view of the separation between the binary components.  $\rho_0=40$  mas is the distance between the Mira and the White Dwarf (WD) and  $\theta_0=130^\circ$  is the position angle of the binary axis (Eyres et al., 2001).  $\theta_I$  are the position angles (at  $45^\circ$  and  $100^\circ$  from the north to the east) of the interferometric baselines from the sky. The thick lines correspond to the projected separations of the binary components on the sky.

- 'HD188512' on page 3
- 'HM Sge' on page 3
- 'HD187642' on page 3
- 'HM Sge' on page 3
- 'HD187642' on page 3
- 'HM Sge' on page 3
- 'HD206778' on page 3
- 'HM Sge' on page 3
- 'HD206778' on page 3
- 'HM Sge' on page 4
- 'HM Sge' on page 4
- 'HM Sge' on page 5
- 'HM Sge' on page 5
- 'HM Sge' on page 5
- 'HM Sge' on page 5
- 'HM Sge' on page 7
- 'HM Sge' on page 8
- 'HM Sge' on page 9
- 'HM Sge' on page 11
- 'R Aqr' on page 11
- 'HM Sge' on page 11
- 'PN M2-9' on page 12
- 'HM Sge' on page 12
- 'HM Sge' on page 12
- 'HM Sge' on page 12
- 'HM Sge' on page 13